Comparison of modular multilevel and flying capacitor converters made of wide bandgap switches for new MVDC grids

Grégoire Le Goff, Ilias Chorfi, Corinne Alonso

ELECTRIMACS 2024 – Castelló de la Plana, Spain, 27-30 May 2024

Comparison of Modular Multilevel and Flying Capacitor Converters Made of Wide Bandgap Switches for New MVDC Grids

Grégoire Le Goff · Ilias Chorfi · Corinne Alonso

Abstract A detailed and comparative analysis of modular multilevel and flying capacitor converters (MMC and, FCC resp.) is proposed in the context of new functionalities developments for new medium-voltage DC (MVDC) grids, taking advantage of the performance and improvement perspectives offered by wide-bandgap (WBG) components. The novelties of this work lie in the generic formalism developed, which enables both structures to be compared on an equal basis, as well as facilitating access to a number of characteristics. This comparison is generalized to the number of phases, number and type of cells, and modulation index. This approach provides a clear overall understanding of the benefits and drawbacks of the two structures in terms of structure sophistication, power conversion capabilities, control complexity, and operating mode freedom. The study highlights the flexibility and the greater power range of the MMC, despite being more complex to control and bulkier than the FCC.

1 Introduction

1.1 WBG multilevel converters to improve MVDC grids

As part of the effort to increase the proportion of renewable energy fed into the grid, increasingly large photovoltaic (PV) farms are being built [13]. This development is accompanied by an increase in the power they can provide to the grid, now reaching new MVDC grids with, for example, DC voltages ranging from 1.5 kV to several tens of kV [2]. At the same time, recent developments have led to the emergence of reliable 650 V wide bandgap (WBG) Galium-Nitride (GaN) components [3]. These novel components offer unique operating performances (low losses, high efficiency, high power density, high switching frequency) which, once integrated into MVDC converters, could see their performance transferred to the scale of the MVDC network, thus improving their overall effectiveness and reaching a lower environmental impact. With a prospective aim of evaluating and quantifying this contribution, the development of converters for the MVDC network is being investigated. To inject energy into the standard European 400 V AC network from an MVDC network using 650 V WBG components, multilevel (ML) topologies are required.

G. Le Goff · I. Chorfi · C. Alonso
LAAS-CNRS - Université de Toulouse, CNRS, UPS
7 Av. du Colonel Roche, 31400 Toulouse, France
e-mail: glegoff@laas.fr, alonsoc@laas.fr, ichorfi@laas.fr

I. Chorfi
STMicroelectronics, Automotive & Discrete Group, CEA Tech

1.2 MMC and FCC: two easy-to-scale-up topologies

Among the various topologies of ML DC/AC converters, two are based on modular structures, enabling them to be built by stacking elementary bricks: the Flying Capacitor Converter (FCC) [14] and the Modular Multilevel Converter (MMC) [11]. A generic representation of these two topologies on an equal basis is shown in Fig. 1. Note that in literature the FCC is also called the multicellular converter.

1.3 Research objective of the work

The objective of this work is to develop modular converters based on WBG components for low MVDC of 1.5kV, and up to medium MVDC of 20kV. To achieve this goal, a detailed comparison of the two modular topologies is needed to provide guidance to ease future design approaches. Although initiated within WBG components and MVDC grid contexts, this comparison is studied to be generic for different active components and applications, as shown in the developments of sections 3 to 6.

1.4 Novelty of the research work

In literature, previous works [4, 6, 15] aim to evaluate losses in both structures. In particular, [6] presents their distribu-

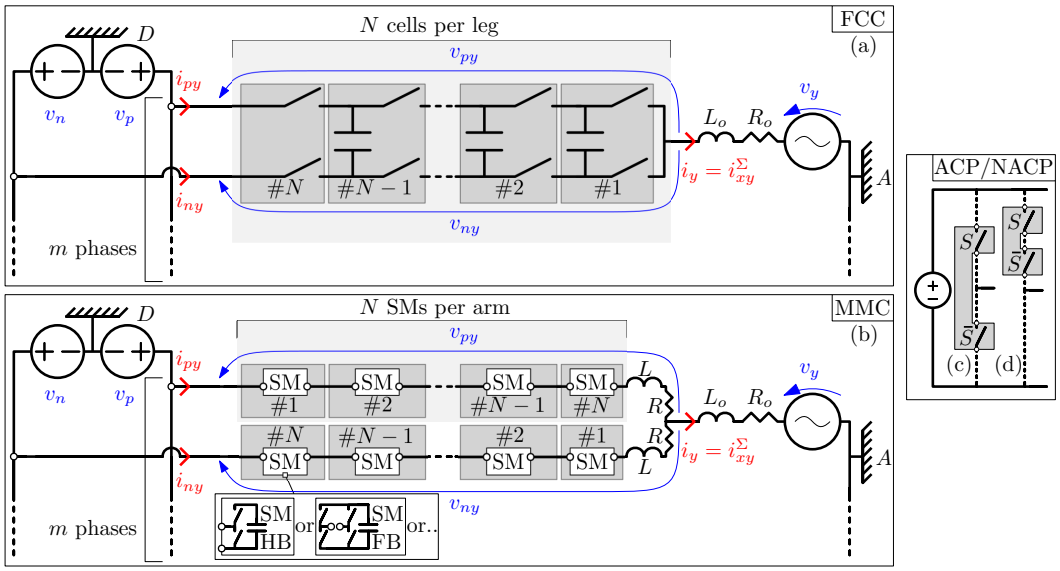

Fig. 1 Generic FCC (a) and MMC (b) topologies with m phases and N switching cells per leg. Switching cell that verifies ACP (c), NACP (d).

tion among switches according to the four operating modes in the (P_{AC}, Q_{AC}) plane. In terms of modeling, the present paper goes into greater detail for both converters, based on the same formalism that enables a readily accessible comparison of additional criteria. The proposed developments are generalized to the number m of phases, N of cells, their type q_j and the modulation index $\bar{m}$, providing a more complete analysis than that of [4, 6, 12, 15].

Some of the study assumptions made by [6, 12] are strong enough to prevent the MMC from being exploited to its full potential. Unlike [4, 6, 15], which do not detail a control law, [12] considers a control architecture in its comparison. But, its current control method does not deal with all currents in the same controller, which can cause problems when saturating control variables. It is very enlightening in terms of co-design, as it proposes a voltage control method that reduces the sizing of passive components. However, it does not take into account the different operating possibilities of the MMC that are detailed here.

The novelty of this work is brought by the generic aspect of the model and its generalization to m, N, $\bar{m}$ and q. It enables a more complete comparison taking into account a number of additional features related to power conversion performance as well as control characteristics in different operating modes for the two structures on an equal basis. This also makes it possible to better understand the two topologies by contrasting them. Also, a novel control architecture based on real-time optimization is implemented, for both converters.

1.5 Outline

After introducing the distinctive property and presenting the generic modeling formalism in Sections 2 and 3 resp., Section 4 presents the real-time optimization control architecture of the two topologies before being implemented for simulations in Section 5. Based on generic modeling, control properties, and simulation results, Section 6 presents their detailed comparison before concluding.

2 Arm-crossing and Non-arm-crossing properties

To analyze DC/AC converter topologies, arm-crossing is one fundamental topological property to highlight. When a converter satisfies the arm-crossing property (ACP), it has switching cells that overlap the two arms of the same converter leg, see Fig. 1(c). Conversely, a converter whose switching cells lie entirely within one arm of the converter verifies the non-arm-crossing property (NACP), see Fig. 1(d).

3 Generic modeling formalism

3.1 Arm currents and voltages

Applying the KIRCHHOFF's voltage law (KVL) to both positive and negative legs of Fig. 1 the following equations are obtained for the MMC as detailed in [9]:

$$\begin{cases} v_{py} = v_p - (v_{AD} + v_y) - \left(Z_o + \frac{Z}{2}\right) i^{\Sigma}_{xy} + \frac{Z}{2} i^{\Delta}_{xy} \\ v_{ny} = v_n - (v_{AD} + v_y) - \left(Z_o + \frac{Z}{2}\right) i^{\Sigma}_{xy} - \frac{Z}{2} i^{\Delta}_{xy} \end{cases} \tag{1}$$

Where y is the leg/phase number, x stands for the arm's DC pole connection, positive ($x = p$) or negative ($x = n$) arm, $i^{\Sigma}_{xy} := i_{py} + i_{ny} = i_y$, $i^{\Delta}_{xy} := i_{py} - i_{ny}$, $Z := R + L\, d/dt$, and $Z_o := R_o + L_o\, d/dt$. v_{AD} is the voltage between neutral points. The same equations are verified by the FCC, except that Z is null. Sum and difference of (1) equations reads:

$$\begin{cases} v^{\Sigma}_{xy} = v_{py} + v_{ny} = v^{\Sigma}_{x} - 2(v_{AD} + v_y) - (2Z_o + Z) i^{\Sigma}_{xy} \\ v^{\Delta}_{xy} = v_{py} - v_{ny} = v^{\Delta}_{x} - Z i^{\Delta}_{xy} \end{cases} \tag{2}$$

Note that Z being null implies v^{Δ}_{xy} to match v^{Δ}_{x} which is V_{DC}. Equation (2) being true for any leg of the converters, it can be generalized to m phases in the AC grid and gathered in

a vector form. In its differential equation version, (2) thus gives:

$$\begin{cases} (2L_o+L)\dot{\mathbf{I}}^{\Sigma} = -(2R_o+R)\mathbf{I}^{\Sigma} - \mathbf{V}^{\Sigma} + \left[\left(v_x^{\Sigma} - 2v_{AD}\right)\mathbf{1} - 2\mathbf{V_y}\right] \\ L\dot{\mathbf{I}}^{\Delta} = -R\mathbf{I}^{\Delta} - \mathbf{V}^{\Delta} + v_x^{\Delta}\mathbf{1} \end{cases} \tag{3}$$

Where $\mathbf{1} := [1,\dots,1]^T \in \mathbb{R}^m$, $\mathbf{I}^{\Sigma} := [i^{\Sigma}_{xy_1},\dots,i^{\Sigma}_{xy_m}]^T \in \mathbb{R}^m$. $\mathbf{I}^{\Delta}$, $\mathbf{V}^{\Sigma}$ and $\mathbf{V}^{\Delta}$ are defined similarly. For the FCC, L and R in (3) are replaced by 0. Should a change of basis be necessary, the following equations enable it:

$$\begin{cases} v^{\Sigma}_{xy} := v_{py} + v_{ny} & v_{py} = \frac{1}{2}\left(v^{\Sigma}_{xy} + v^{\Delta}_{xy}\right) \\ v^{\Delta}_{xy} := v_{py} - v_{ny} & v_{ny} = \frac{1}{2}\left(v^{\Sigma}_{xy} - v^{\Delta}_{xy}\right) \end{cases} \tag{4}$$

Thus, in its vector form (4) reads: $\mathbf{V}^{\Sigma} = \mathbf{V}_{py} + \mathbf{V}_{ny}$ and $\mathbf{V}^{\Delta} = \mathbf{V}_{py} - \mathbf{V}_{ny}$. Same is true for the currents $\mathbf{I}^{\Sigma}$ and $\mathbf{I}^{\Delta}$. The connection function of the N-th cell of the FCC gives the average value model $i_{py} = D_{y\,N}\, i^{\Sigma}_{xy}$ and, by complementarity $i_{ny} = (1-D_{y\,N})i^{\Sigma}_{xy}$. The duty cycle of the mentioned cell is noted $D_{y\,N}$. Consequently, a link, valid only for the FCC, is established between i^{Σ}_{xy} and i^{Δ}_{xy}:

$$i^{\Delta}_{xy} = (2D_{y\,N} - 1)i^{\Sigma}_{xy} \tag{5}$$

3.2 Arm voltages, capacitor voltages and duty cycles

Applying the KVL to each positive and negative arm of the MMC, gives the following equation:

$$\begin{cases} v_{py} = \mathbf{V}^T_{\mathbf{Cpy}}\mathbf{D_{py}} \\ v_{ny} = -\mathbf{V}^T_{\mathbf{Cny}}\mathbf{D_{ny}} \end{cases} \tag{6}$$

Both equations can be summarized into $v_{xy} = \sigma(x)\mathbf{V}^T_{\mathbf{Cxy}}\mathbf{D_{xy}}$. Where $\mathbf{V_{Cxy}} := [v_{C_{xy\,1}},\dots,v_{C_{xy\,N}}]^T \in \mathbb{R}^N$ is the vector of all capacitor voltages in arm #xy of the MMC. The vector $\mathbf{D_{xy}}$ is defined similarly from the N duty cycles of the submodules (SMs). All duty cycles $D_{xy\,j}$ are limited to $[1-q_j;1]$. With $q_j = 1$ if the considered SM is a half-bridge (SM-HB), and $q_j = 2$ in the full-bridge (SM-FB) case. The subscript $j \in [\![1;N]\!]$ stands for the SM index. The function $\sigma(x)$ is 1 for $x = p$ and -1 for $x = n$. Similarly, the application of the KVL to the FCC shows that:

$$\begin{cases} v_{py} = \mathbf{V}^T_{\mathbf{Cell_y}}(\mathbf{1}-\mathbf{D_y}) = V_{DC} + v_{ny} \\ v_{ny} = -\mathbf{V}^T_{\mathbf{Cell_y}}\mathbf{D_y} = -D_{y\,N}V_{DC} - \sum_{j=1}^{N-1} v_{C_{y\,j}}(D_{y\,j} - D_{y\,j+1}) \end{cases} \tag{7}$$

Where $\mathbf{V_{Cell_y}} := [v_{C_{y\,1}}, v_{C_{y\,2}} - v_{C_{y\,1}},\dots,V_{DC} - v_{C_{y\,N-1}}]^T \in \mathbb{R}^N$ is the vector of all cell voltages in leg #y of the FCC and j is the cell index. The vector $\mathbf{D_y}$ is defined similarly from the N duty cycles of the cells. All $D_{y\,j}$ are limited to $[0;1]$. Sum and difference of (6) equations reads, for the MMC:

$$\begin{cases} v^{\Sigma}_{xy} = \mathbf{V}^T_{\mathbf{Cpy}}\mathbf{D_{py}} - \mathbf{V}^T_{\mathbf{Cny}}\mathbf{D_{ny}} \\ v^{\Delta}_{xy} = \mathbf{V}^T_{\mathbf{Cpy}}\mathbf{D_{py}} + \mathbf{V}^T_{\mathbf{Cny}}\mathbf{D_{ny}} \end{cases} \tag{8}$$

Likewise, the following is obtained for the FCC from (7):

$$\begin{cases} v^{\Sigma}_{xy} = v_{py} + v_{ny} = V_{DC} - 2\mathbf{V}^T_{\mathbf{Cell_y}}\mathbf{D_y} \\ v^{\Delta}_{xy} = v_{py} - v_{ny} = V_{DC} \end{cases} \tag{9}$$

Applying OHM's and KIRCHHOFF's current laws to any capacitor of the MMC shows that:

$$\forall j \in [\![1;N]\!]\ \dot{v}_{C_{xyj}} = \frac{\sigma(x)i_{xy}}{C}S_{xyj} \Longrightarrow \dot{\mathbf{V}}_{\mathbf{C_{xy}}} = \frac{\sigma(x)i_{xy}}{C}\mathbf{D_{xy}} \tag{10}$$

For the FCC, capacitor current depends on the difference between currents flowing through the neighboring switches:

$$\forall j \in [\![1;N-1]\!]\ \dot{v}_{C_{yj}} = \frac{i^{\Sigma}_{xy}}{C}(S_{y\,j+1} - S_{y\,j}) \Longrightarrow \dot{\mathbf{V}}_{\mathbf{C_y}} = \frac{i^{\Sigma}_{xy}}{C}\tilde{M}_N\mathbf{D_y} \tag{11}$$

$$\tilde{M}_N := \begin{bmatrix} -1 & 1 & & \\ & -1 & 1 & \\ & & \ddots & \ddots \\ & & & -1\ \ 1 \end{bmatrix} \in \mathbb{R}^{N-1\times N}$$

Where $S_\bullet$ are the switching states transformed into duty cycles $D_\bullet$ when considering the average value model at the scale of the switching period. Applying the KVL to each SM gives the maximum voltage that each switch will face:

$$\forall j \in [\![1;N]\!]\ \hat{v}_{sw_{xyj}} = v_{C_{xyj}} \Longrightarrow \text{Nominal: } \hat{v}_{sw_{xyj}} = v_C^{nom} \tag{12}$$

The same is done for the FCC cells, which leads to:

$$\forall j \in [\![1;N]\!]\ \hat{v}_{sw_{yj}} = v_{Cell_{yj}} \Longrightarrow \text{Nominal: } \hat{v}_{sw_{yj}} = V_{DC}/N \tag{13}$$

In the last cell, it comes $\hat{v}_{sw_{yN}} = v_{Cell_{yN}} = V_{DC} - v_{C_{y\,N-1}}$, and there is $\hat{v}_{sw_{yj}} = v_{Cell_{yj}} = v_{C_{y\,j}} - v_{C_{y\,j-1}}$. Thus, in order to have the same rating for all switches, it comes by mathematical induction that $v_{Cell_{yj}}$'s nominal voltage should be V_{DC}/N, hence (13).

3.3 Powers and energies

The power flowing through each arm of the MMC is directly derived from the corresponding voltages and currents $p_y = p_{py} + p_{ny} = v_{py}i_{py} + v_{ny}i_{ny}$:

$$p_y = \left[\frac{V_{DC}}{2}i^{\Delta}_{xy} - \frac{Z}{2}i^{\Delta^2}_{xy}\right] - \left[(v_{AD}+v_y)i^{\Sigma}_{xy} + \left(\frac{Z}{2}+Z_o\right)i^{\Sigma^2}_{xy}\right] \tag{14}$$

The same is true for the FCC when Z is replaced by 0:

$$p_y = \left[\frac{V_{DC}}{2}i^{\Delta}_{xy}\right] - \left[(v_{AD}+v_y)i^{\Sigma}_{xy} + Z_o i^{\Sigma^2}_{xy}\right] = -\frac{\tilde{\mathbf{V}}^T_{\mathbf{Cell_y}}}{2}T_R\, C\dot{\mathbf{V}}_{\mathbf{C_y}} \tag{15}$$

Where $\tilde{\mathbf{V}}_{\mathbf{Cell_y}}$ is such that $\mathbf{V}_{\mathbf{Cell_y}} := [\tilde{\mathbf{V}}^T_{\mathbf{Cell_y}}, V_{DC} - v_{C_{y\,N-1}}]^T \in \mathbb{R}^N$ and T_R is the upper right triangular $N-1 \times N-1$ matrix filled with 1's. By inverting the linear system made of the $N-1$ equations contained in (11) and the equation of v^{Σ}_{xy} from (7), together, it is possible to derive the N duty cycles of which $D_{y\,N}$ is a part. The expression thus obtained can be used to substitute $D_{y\,N}$ in (5). The resulting formula for i^{Δ}_{xy} is used to substitute i^{Δ}_{xy} in the expression of p_y. This gives p_y as a function of $\dot{\mathbf{V}}_{\mathbf{C_y}}$ according to (15) for the FCC.

4 Control architectures

The design of the control architectures implemented here is driven by the aim to compare structures on their full operating regions. Nevertheless, they are based on the specific operating principle of each topology, as described in Fig. 2.

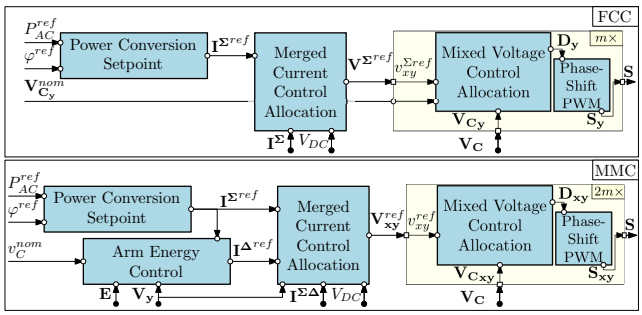

Fig. 2 Control allocation-based MMC and FCC control architectures

4.1 MMC control

NACP allows v_{py} to be independent of v_{ny}, as shown by (6), so v^{Δ}_{xy} is free with respect to V_{DC}, see (8). Giving the MMC more current control (CC) freedom than the FCC. So, as (3) points out, the current i^{Δ}_{xy} is controllable in the MMC, which gives more energy control (EC) freedom. Choosing to suppress the circulating current (CCS) reduces losses and extends the operating power range, but modifies the energy balancing quality when compared to circulating current injection (CCI).

For CC, it is necessary to provide reference tracking for i^{Δ}_{xy} in addition to i^{Σ}_{xy}, the latter representing the AC grid current. There will therefore be $2m$ currents to control and $2m$ voltages (v_{py} and v_{ny}) to do so. Previous work of [7] proposes novel control allocation (CA) approaches to take advantage of each of these voltages in order to control all currents from a single controller in a merged and optimized fashion, while taking into account control constraints a priori. This approach can be augmented by a transparent integral compensator [8] depending on the desired performance.

For voltage control (VC), the aim is to keep track of the v_{py} and v_{ny} references imposed by the current loop. According to (6), there are N duty cycles to control a single voltage. So there is an infinite number of solutions. An optimization is implemented with the primary objective of minimizing the difference between v_{xy} and their references. In order to guide the optimization to choose one of the multiple candidate solutions, a secondary criterion is taken into account: minimizing the deviation between the N capacitor voltages $v_{C_{xyj}}$ and their nominal value, since duty cycles also influence the capacitor voltage (10). [10] presents this CA approach, where $2m$ optimizations are performed in parallel, one for each arm of the converter, to ensure arm and capacitor voltage control simultaneously.

4.2 FCC control

The ACP leads to v_{py} being dependent on v_{ny} as shown by (7), so v^{Δ}_{xy} is equal to V_{DC} permanently, see (9). Reducing the FCC current control freedom, compared to the MMC. Thus, as (5) points out, the current i^{Δ}_{xy} is not controllable since $D_{y\,N}$ is determined to track the reference of the current i^{Σ}_{xy}, and i^{Σ}_{xy} follows its reference. As a result, the energy balance of the legs, $p_y = 0$, is naturally assured as long as capacitor balancing is guaranteed (15), and EC does not need to be implemented, unlike for the MMC.

For CC, it is therefore necessary to provide reference tracking for i^{Σ}_{xy} only, that is m currents to control from m voltages, i.e. half as much as for the MMC. To achieve this, conventional methods for controlling AC currents in an electrical system can be implemented. However, to improve the control performances and have an approach comparable to that of the MMC with CA methods, the latter can also be applied here. Without going into detail, they are mainly based on the concepts presented in [8].

For VC, the aim is to keep track of v^{Σ}_{xy} references. According to (7) there are N duty cycles to control a single voltage. So, as with the MMC, a CA implementing real-time optimization is set up with a primary criterion of v^{Σ}_{xy} reference tracking and a secondary criterion of $v_{C_{yj}}$ capacitor balancing around their nominal value.

The development of control allocation (CA) methods in electrical engineering [1, 5, 7] is a recent topic that remains to be explored. Allowing control efforts to be distributed in an optimized manner while taking constraints into account a priori, they offer perspectives with the potential to have a major impact on the operation of electrical systems.

5 Simulation testing procedure

In order to highlight the conversion capabilities of both topologies, the same tests are carried out in simulation. The control architecture implemented described by Fig. 2 takes power setpoints as input. These setpoints follow the profile described by Fig. 3 in order to trigger the following converter behaviors: 1) power ramp-up to nominal, 2) steady-state behavior, 3) transient behavior, 4) all power factor possibilities (round cycle in the (P_{AC}, Q_{AC}) frame). Simulations are carried out with Matlab-Simulink, implementing detailed converter models using the PLECS Blockset. The detailed losses

Quantity	Networks	
DC bus voltage V_{DC}	1.5 kV	
AC grid voltage $\hat{V}_{AC}$ amplitude	$\sqrt{2}\cdot 230 \simeq 327$ V	
AC grid frequency f_{AC}	50 Hz	
Modulation index $\bar{m}$	0.434	
Quantity	Semiconductors	
Voltage rating $\hat{v}_{sw}$	650 V (used at 400 V for margin)	
Current rating $\hat{i}_{sw}$	7.07 A	
Switching frequency f_s	100 kHz	
Quantity	MMC	FCC
No. of phases or legs m	1	1
No. of cells/leg or SMs/arm N	4	4
Cells or SMs capacitor C	414 mF	0.7 μF
Arm inductor L	6.1 mH	None

Table 1 Simulation parameters - MMC vs. FCC

Quantity	MMC	FCC
Voltage v_{xy} range	qV_C^Σ	V_{DC}
Voltage range flexibility	Yes $(= f(V_C^\Sigma))$	No $(= f(V_{DC}))$
Power range for $\bar{m}=1$	1 to 1.30 p.u.	1 p.u.
Power range for $\bar{m}=2$	1.34 to 1.95 p.u.	unreachable
Efficiency (simul. mean)	96.50%	97.64%

Table 2 Energy conversion perf. characteristics - MMC vs. FCC

model of the GaN switches is obtained through meticulous experimental electrical and thermal data measurement, enabling high-accuracy simulation of losses. The Fig. 3 shows that AC grid power reference tracking is ensured for both converters on all four quadrants of the (P_{AC}, Q_{AC}) plane. It can be seen that over the simulated operating conditions, the efficiency of the FCC is slightly better than that of the MMC. According to Fig. 4, the FCC is about 1.14% more efficient than the MMC on average.

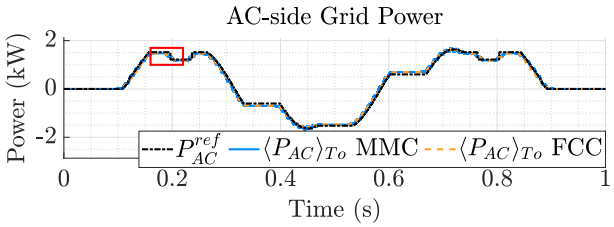

Fig. 3 Power delivered to the AC grid.

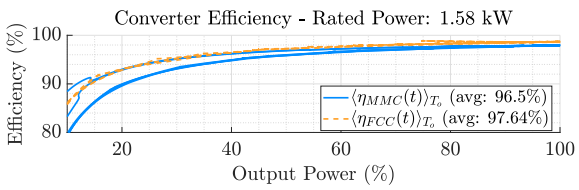

Fig. 4 Efficiency of the converters on the 10% to 100% power range

6 Comparison of the topologies

6.1 Energy conversion performance

As (12) and (13) show, the maximum voltage that the switches will handle is deduced. Based on (6), the $\sigma(x)v_{xy}$ will reach $V_C^\Sigma := \sum_j v_{C_{xyj}}$ at maximum and $(1-q)V_C^\Sigma$ at minimum for

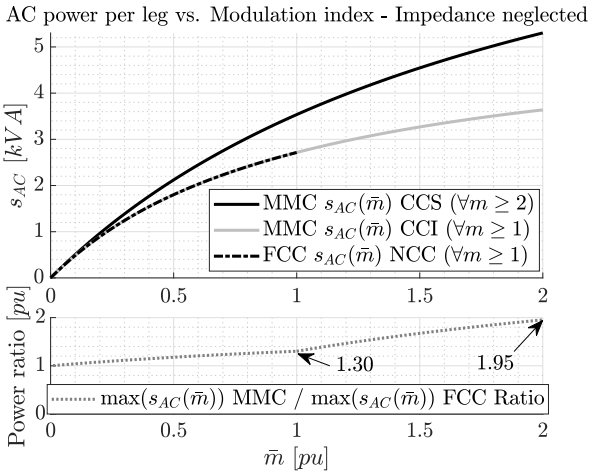

Fig. 5 Power range of both topologies as a function of $\bar{m}$

the MMC, i.e. a range of qV_C^Σ, against a voltage between 0 and V_{DC}, i.e. a range of V_{DC}, for the FCC according to (7).

According to (15) and (14), $p_y = \frac{V_{DC}}{2} i_{xy}^\Delta - v_y i_{xy}^\Sigma$ for both converters. In steady state $p_y = 0$, this allows us to derive i_{xy}^Δ for a given i_{xy}^Σ, V_{DC} and $\hat{V}_{AC}$ (v_y's amplitude). It is shown that i_{xy}^Δ has a DC and AC component at $2f_{AC}$ (corresponding to CCI for the MMC, but natural circulating current (NCC) for the FCC). Given V_{DC}, i_{xy}^Σ, $\hat{V}_{AC}$ and a semiconductor current limit, it is possible to derive the maximum power that each leg can convert as a function of $\bar{m} = 2\hat{V}_{AC}/V_{DC}$. As the FCC is constrained to run the current i_{xy}^Δ satisfying $p_y = 0$ in steady state, this current is not controllable for it which satisfies the ACP. Whereas the MMC, verifying the NACP, will be able to impose some other value to the current i_{xy}^Δ. In particular, to ensure global energy balancing of the MMC, it is possible to determine i_{xy}^Δ to ensure $\sum_y p_y = 0$ instead of $p_y = 0$. This leads to the cancellation of the AC component of i_{xy}^Δ (CCS) for $m > 1$. The Fig. 5 shows the evolution of the convertible power per leg as a function of $\bar{m}$ and the control strategy. By canceling out the AC component of i_{xy}^Δ, part of the range of v_{py} and v_{ny} will be freed up, enabling larger i_{xy}^Σ currents to be reached. Thus, for $\bar{m} = 1$, the MMC can convert around 30% more power than the FCC. Since the modulation range of the MMC can go beyond that of the FCC by using some SM-FBs ($\bar{m} = 2$), the MMC can convert up to 95% more power than the FCC.

Since the MMC has more active components than the FCC, as well as $2m$ more inductors, it is likely to have more losses. However, according to Fig. 4, this comparison gives here a 1.14% better efficiency on average for the FCC.

6.2 Power conversion control

The operating range of the FCC depends directly on V_{DC} (see Tab. 2): a change in bus voltage instantly and permanently alters the operating range, making it impossible to convert the same current and therefore the same power. On the other hand, if V_{DC} varies, the MMC - whose operating

Quantity	MMC	FCC
EC Necessity	Yes	No
Minimum control architecture	EC+CC+VC	VC
Number of currents to control (Number of EC degrees of freedom)	$2m$	m
Number of voltages to control (Number of CC degrees of freedom)	$2m$	m
Freedom of energy balancing	Yes	No
Freedom to reduce arm losses according to control strategy	Yes	No
Resilience to DC voltage variations	Yes	No

Table 3 Power conversion control characteristics - MMC vs. FCC

range depends on V_C^{Σ} - continues to maintain the same operating zone. Tab. 3 summarizes the comparison criteria of this section and those already available in Section 4.

7 Conclusions

This study, comparing the operating capabilities of the MMC and the FCC, will help guide future choices and design approaches for multilevel converters that feature a modular property, depending on the targeted application. For instance, the FCC is less bulky and has a higher efficiency. Its power conversion capabilities are both rigid and reduced, but its control architecture is simpler. The NACP provides the MMC with operating freedoms unavailable to the FCC. This operating freedom also enables the MMC to convert up to 30% more power, when the circulating currents are suppressed.

Also, the advanced control methods used in this study enable new functionalities for both converters, such as the ability to optimally distribute the control effort among the different cells, or the ability to wisely manage saturations of control variables.

Based on the work presented here, a realization of both converters using WBG components is part of the future work with a comparative study based on experimental results. This aims to enable sound design methods for both topologies made from WBG components.

References

[1] A. Bouarfa et al. “A new control allocation method for power converters and its application to the four-leg two-level inverter”. In: *2015 23rd Mediterranean Conference on Control and Automation (MED)*. 2015, pp. 1020–1026.

[2] Y. Chen et al. “Techno-Economical Comparison of MVAC and MVDC Micro-Grids with High PV Penetration”. In: *2023 IEEE PES Grid Edge Technologies Conference & Exposition (Grid Edge)*. 2023, pp. 1–5.

[3] I. Chorfi et al. “A GaN-Based Three-Level Dual Active Half Bridge Converter With Active Cancellation of the Steady-State DC Offset Current”. English. In: *IECON 2022 – 48th Annual Conference of the IEEE Industrial Electronics Society*. 2022.

[4] D. Jiao et al. “Evaluation of Medium Voltage SiC Flying Capacitor Converter and Modular Multilevel Converter”. In: *2020 IEEE Energy Conversion Congress and Exposition (ECCE)*. 2020, pp. 4386–4392.

[5] J. Kreiss. “Allocation de commande pour l’électrotechnique et l’électronique de puissance”. fr. PhD thesis. Université de Lyon, 2019.

[6] P. Ladoux et al. “Comparison of high voltage modular AC/DC converters”. In: *Automation and Motion International Symposium on Power Electronics Power Electronics, Electrical Drives*. 2012, pp. 843–848.

[7] G. Le Goff. “Scalable Control Allocation Methods for the Modular Multilevel Converter: from Modelling to Real Time Implementation”. en. PhD Thesis. Institut National Polytechnique de Toulouse (INPT), 2022.

[8] G. Le Goff et al. “Model Reference Control of Constrained Overactuated Systems with Integral Compensation”. In: *2022 IEEE 61st Conference on Decision and Control (CDC)*. 2022, pp. 4507–4512.

[9] G. Le Goff et al. “Scalable Control-Oriented Model of the Modular Multilevel Converter for Polyphase Systems”. In: *IEEE Transactions on Industry Applications (TIA)* 58.3 (2022), pp. 4050–4061.

[10] G. Le Goff et al. “Scalable Optimal Control Allocation: Linear and Quadratic Programming Methods Applied to Active Capacitor Balancing in Modular Multilevel Converters”. en. In: *IFAC-PapersOnLine* 55.16 (2022), pp. 80–85.

[11] R. Marquardt. “Current rectification circuit for voltage source inverters with separate energy stores replaces phase blocks with energy storing capacitors”. en. DE10103031A1. 2002.

[12] S. C. Mersche et al. “Comparison of Quasi-Two-Level Operation of a Flying Capacitor Converter with Quasi-Two-Level Operation of a Modular Multilevel Converter”. In: *2022 IEEE 7th Southern Power Electronics Conference (SPEC)*. ISSN: 2832-2983. 2022, pp. 1–6.

[13] P. L. Métayer et al. “Phase-Shifted Full Bridge DC–DC Converter for Photovoltaic MVDC Power Collection Networks”. In: *IEEE Access* 11 (2023). Conference Name: IEEE Access, pp. 19039–19048.

[14] T. A. Meynard et al. “Multilevel conversion: high voltage choppers and voltage-source inverters”. In: *PESC ’92 Record. 23rd Annual IEEE Power Electronics Specialists Conference*. 1992, 397–403 vol.1.

[15] T. Younis et al. “Three-Phase Multilevel Inverters for LV Systems: Comparison of Modular Multilevel Converter and Flying Capacitor Structures”. In: *2023 IEEE Conference on Power Electronics and Renewable Energy (CPERE)*. 2023, pp. 1–5.